Evaluating the C, N, and F Pairwise Codoping Effect on the Enhanced Photoactivity of ZnWO4: The Charge Compensation Mechanism in Donor–Acceptor Pairs

ARTICLE *in* THE JOURNAL OF PHYSICAL CHEMISTRY C · JULY 2011

Impact Factor: 4.77 · DOI: 10.1021/jp204324n

7 AUTHORS, INCLUDING:

Xian Zhao
Shandong University
239 PUBLICATIONS **2,023** CITATIONS
SEE PROFILE

Yanlu Li
Universität Paderborn
29 PUBLICATIONS **242** CITATIONS
SEE PROFILE

Pan Li
Hebei Normal University
24 PUBLICATIONS **298** CITATIONS
SEE PROFILE

Weiliu Fan
Shandong University
79 PUBLICATIONS **1,435** CITATIONS
SEE PROFILE

THE JOURNAL OF PHYSICAL CHEMISTRY C

ARTICLE

pubs.acs.org/JPCC

Evaluating the C, N, and F Pairwise Codoping Effect on the Enhanced Photoactivity of $ZnWO_4$: The Charge Compensation Mechanism in Donor−Acceptor Pairs

Liming Sun,[†] Xian Zhao,[‡] Xiufeng Cheng,[‡] Honggang Sun,[‡] Yanlu Li,[‡] Pan Li,[‡] and Weiliu Fan*[,†]

[†]Department of Chemistry and Chemical Engineering, Shandong University, Jinan 250100, China

[‡]State Key Laboratory of Crystal Materials, Shandong University, Jinan 250100, China

Supporting Information

ABSTRACT: We perform first-principles density function theory calculations to study the geometric and electronic structures and photoactivity of C, N, and F monodoped and pairwise codoped $ZnWO_4$. By incorporating single C, N, or F into $ZnWO_4$, considering substitutional as well as interstitial locations of dopants in the $ZnWO_4$ lattice, we find that the photon transition energy decreases to varying degrees, while the partially occupied states induced by the impurity are located in the gap, which may act as recombination centers and reduce the photoinduced current density. By analyzing the defect wave function character, we propose several pairwise codoped $ZnWO_4$ systems, such as C_s+2F_s-, N_s+F_s-, C_i+2N_s-, and N_i+F_s-codoped $ZnWO_4$, to passivate the partially occupied states in the monodoping systems by the charge compensation effect in the donor−acceptor pairs, resulting in occupied states in the gap and reducing the formation energy compared with the monodoping systems. The C_s+2F_s and N_s+F_s codoping do not narrow the host band gap of $ZnWO_4$, while they decrease the excitation energy from the occupied gap states to the conduction band minimum to some extent. The C_i+2N_s and N_i+F_s codoping in the $ZnWO_4$ can red shift the transition energy of photoexcited electrons from the impurity levels to the conduction band minimum to the ideal visible-light region; therefore, the C_i+2N_s codoping can decrease the host band gap of $ZnWO_4$ by about 0.3 eV. Our results show that the partially occupied states in the monodoping $ZnWO_4$ can be passivated by the charge compensation effect in the donor−acceptor pairs, thus improving the photoactivity and reaching the visible-light photoactivity for $ZnWO_4$.

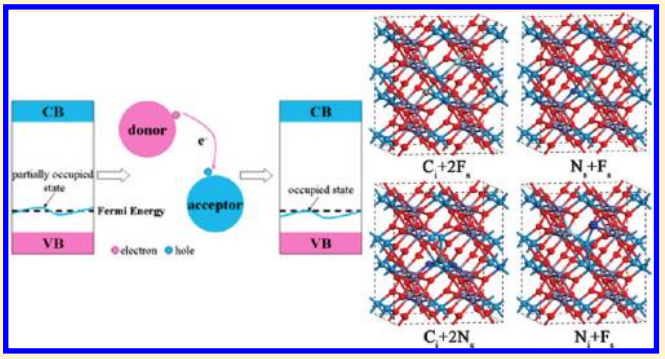

1. INTRODUCTION

In the past decades, energy shortage and environmental deterioration have become the major obstacles to the development of economy and society. Semiconductor photocatalysts have attracted much attention, owing to their applications to environmental purification and solar energy conversion.[1−3] TiO_2-based materials, doping with metals and nonmetals, have been intensively investigated as promising photocatalysts.[4−14] More recently, exploring new types of photocatalysts except TiO_2 has become a crucial subject for energy source and environment science and technology.

As part of the tungstate family, $ZnWO_4$ has been used for mineralization of organic pollutants under UV light irradiation. However, the $ZnWO_4$ industrial application is hampered because the photocatalytic activity of $ZnWO_4$ is not high enough for the requirements of practical applications.[15−17] Zhu et al. have introduced fluorine anions into the $ZnWO_4$ substrate to solve this disadvantage, and their experiments have shown promising photocatalytic activity for F-$ZnWO_4$ under UV light illumination.[18,19] In our previous experimental work, the interstitial F-doped $ZnWO_4$ nanostructure has achieved better photocatalytic activity with UV radiation.[20] From the further theoretical research, we found that there are two different photocatalytic mechanisms in the F substituted O-doped and interstitial F-doped $ZnWO_4$, both of which show promising photocatalytic activity.[21] However, two problems are still not resolved in the F-doped $ZnWO_4$ system. One problem is that the photogenerated current of F-doped $ZnWO_4$ under UV radiation may not be high enough because partially occupied states located in the band gap tend to trap photogenerated electrons, thereby reducing the photogenerated current. Another problem is that F-doped $ZnWO_4$ allows only absorption of UV irradiation, which amounts to ∼5% of solar energy. To overcome the above inconveniences, a possible way to improve the photoactivity performance of $ZnWO_4$ is to exploit the cooperative effect of introducing different dopants into the matrix, because the defect bands are passivated and they will not be active as carrier recombination centers. Though the "codoping effect" is actually receiving noticeable attention,[22−34] codoping is

Received: May 9, 2011
Revised: June 30, 2011
Published: July 05, 2011

not a guarantee of successful efficient visible photocatalysts,[25,26] indicating that a careful analysis and evaluation of the choice of codopants is important.

Semiconductor photocatalysis doping with transition metals has some problems, such as thermal instability and an increase of charge carrier recombination centers; thus, the application is limited for efficient photocatalytic reactions.[35,36] Doping of nonmetal anions in the semiconductors has been proven to be very promising for efficient photocatalytic oxidation of organic compounds under visible-light radiation.[10,37] The valence band maximum state of pure $ZnWO_4$ consists mostly of the O 2p orbital. Therefore, to have a red shift of the $ZnWO_4$ adsorption edge, the anions should have a higher p orbital energy than O 2p; that is, it should be weaker electronegatively than the O atom. Simple electron counting suggests that C and N ideally fulfill the aforementioned requirements. Another important demand for improving the photoactivity of $ZnWO_4$ is that the electrons on the donor levels passivate the same amount of holes on the acceptor levels, in order to keep the semiconductor character of the system. Therefore, we anticipate that good codopants chosen in C, N, and F atoms can lead to a semiconducting system with higher photoactivity not only under UV radiation but also in the visible-light region than pure $ZnWO_4$. There have been several publications reporting on successful fabrication of codoped photocatalysts, such as TiO_2[27−29,31,38] and ZnS.[39,40]

In the present paper, we examined the microscopic electronic structure of C, N, and F monodoped and pairwise codoped $ZnWO_4$ to explore the synergistic effects of the dopants in detail. We have fabricated appropriate C-doped, N-doped, F-doped, (C, F)-codoped, (C, N)-codoped, and (N, F)-codoped models and carried out a comparative analysis of geometric and electronic structures by means of a first-principles density functional theory (DFT) method. On the basis of our calculations, the mechanisms of improving the photoactivity of $ZnWO_4$ are illuminated from the point of view of so-called donor−acceptor pairs (DAP) recombination.[41] Theoretical investigations provide detailed microscopic information on the electronic structure of the system and are therefore useful to identify a "good pair" of dopants with potential synergistic effects. We expected that this knowledge would aid the further design and construction of new effective visible-light photocatalysts.

2. COMPUTER DETAILS AND STRUCTURE ASPECTS

On the basis of first-principles density function theory (DFT), calculations were performed using the Cambridge Sequential Total Energy Package (CASTEP)[42] program package. As shown in our previous work,[20,21] the exchange-correlation functional was described by a generalized gradient approximation (GGA)[43] with the Perdew−Burke−Ernzerhof (PBE)[44] scheme. Interaction between the valence electrons and ion core was substituted by an ultrasoft pseudopotential.[45] The pseudopotentials for Zn, W, O, C, N, and F atoms represented $3d^{10}4s^2$, $5s^25p^65d^46s^2$, $2s^22p^4$, $2s^22p^2$, $2s^22p^3$, and $2s^22p^5$, respectively. Electronic wave functions were expanded in terms of a discrete plane wave basis set. To achieve the accurate density of the electronic states, the *k*-space integrations were done with Monkhorst−Pack grids[46] with a $5 \times 4 \times 5$ *k*-point in the Brillouin zone of the monoclinic $ZnWO_4$. Before the single-point energy calculation, geometry optimization was done, and the self-consistent convergence accuracy was set at 1×10^{-5} eV/atom, the convergence criterion for the force between atoms was 3×10^{-2} eV/Å, and the maximum displacement was 1×10^{-3} Å.

On the basis of the optimized geometry, a $2 \times 2 \times 2$ $ZnWO_4$ crystal cell was employed to construct the doped configuration, corresponding to a 96-atom supercell. For monodoping systems, substitutional as well as interstitial locations of C, N, and F atoms in the $ZnWO_4$ lattice were both considered, which is labeled with the subscript of s and i, respectively. There are two different oxygen atoms in the $ZnWO_4$ crystal. O_a is bonded to two tungsten atoms and one zinc atom, and O_b is bonded to two zinc atoms and one tungsten atom. Therefore, two different substitutional sites were considered, and our calculations indicated that C, N, and F atoms substituted to the O_a site were the most stable structures. Several originally interstitial sites of these atoms were also taken into account, and only the structures of the lowest energy were considered in the present discussion. For codoping systems, on the basis of the discussions for monodoped $ZnWO_4$ and the electronic configurations of C $2s^22p^2$, N $2s^22p^3$, and F $2s^22p^5$, we think that $2C_s$+F_s, C_i+$2N_s$, N_s+F_s, N_s+F_i, N_i+F_s, and N_i+F_i codoping as codopant pairs probably achieve a desirable photoactivity. For all the doped structures, the geometrical optimization was implemented at the Γ point, and a $3 \times 2 \times 3$ *k* mesh was used for electronic property calculations based on the corresponding optimized geometries. The spin polarization effect had been taken into account in our calculations for the electronic structures of monodoping and codoping systems.

To compare the relative stability of monodoping and codoping systems, we calculated the formation energies of the doped $ZnWO_4$ supercell according to the following formulas

$$E_f = E_{tot}(defect) - E_{tot}(pure) - n_C\mu_C - n_N\mu_N - n_F\mu_F + n_O\mu_O$$

Here, E_{tot}(defect) is the total energy of the supercell with doping and E_{tot}(pure) is the total energy of the ideal supercell. n_C, n_N, and n_F are the number of C, N, and F doping in the lattice of $ZnWO_4$. n_O is the number of O atoms being removed from the supercell, which is one for monosubstituted doping, two for double-substituted doping, three for triple-substituted doping, and zero for interstitial doping. μ_C, μ_N, μ_F, and μ_O represent the chemical potential of the C, N, F, and O atoms. It should be mentioned that the formation energy is not fixed but depends on the growth condition, which can be O-rich, O-poor, or anything in between. The μ_N and μ_F is fixed at the energy of half an N_2 and an F_2 molecule, respectively. The chemical potential of C (μ_C) is calculated according to $C+O_2 \rightarrow CO_2$, and μ_{CO_2} is equal to the energy of one CO_2 molecule. Under O-rich conditions, μ_O is equal to the energy of half an O_2 molecule. Under O-poor conditions, μ_O is calculated as

$$Zn + W + 2O_2 \rightarrow ZnWO_4 + \Delta H$$

where μ_{Zn} and μ_W are fixed at the energy of bulk Zn and W per atom, respectively, and ΔH is the heat of $ZnWO_4$ formation (−14.56 eV). The calculated energy of μ_O is fixed at $^1/_2\mu_{O_2}$ −3.64 eV in the O-poor limit.

3. RESULTS AND DISCUSSION

3.1. Mono C-, N-, or F-Doped $ZnWO_4$. A useful prerequisite for understanding cooperative effects in codoping is the precise knowledge of the separately doped systems. In this section, we have investigated a variety of configurations of mono C, N, or F

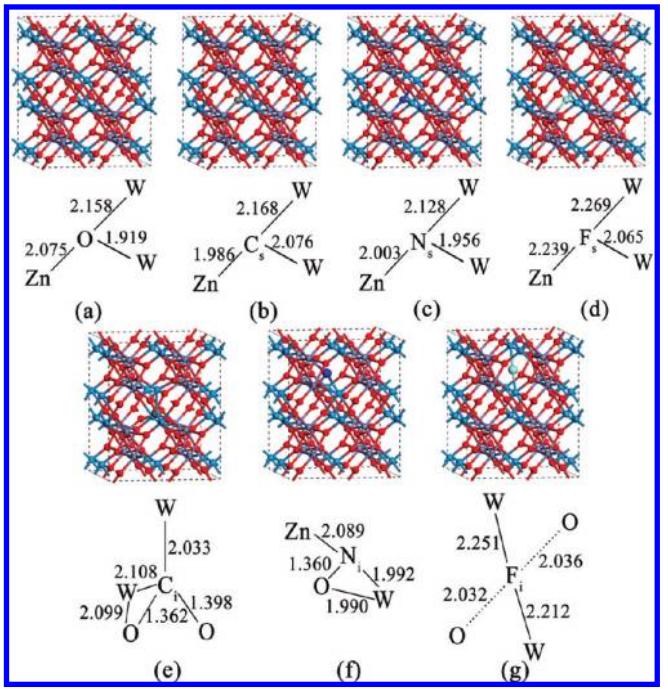

Figure 1. The optimized structures of (a) pure, (b) C_s-doped, (c) N_s-doped, (d) F_s-doped, (e) C_i-doped, (f) N_i-doped, and (g) F_i-doped $ZnWO_4$. The partial structures are also shown. The gray, azure, red, dark gray, blue, and pewter spheres represent zinc, tungsten, oxygen, carbon, nitrogen, and fluorine, respectively.

located at substituted and interstitial positions in the $ZnWO_4$ supercell. Our main aim is studying the changes of the local microstructures and the electronic structures due to the doping atom and further to discuss whether the changes can red shift the adsorption edge and improve the photoactivity of $ZnWO_4$.

A. Geometric Structures. Figure 1 illustrates the optimized geometric structures of pure and mono C-, N-, and F-doped $ZnWO_4$. For the monosubstituted structures (Figure 1b–d), the whole structural variations following O replacement with C, N, and F are found to be a slight change after geometry optimization. According to our calculations, the lengths of Zn–X (X = C, N, O, and F) bonds can be ordered as follows: Zn–C (1.986 Å) < Zn–N (2.003 Å) < Zn–O (2.075 Å) < Zn–F (2.239 Å), which should be contributed to the more valence electrons causing the larger Coulomb repulsion between the Zn and X atoms. The optimized W–X (X = C, N, and F) bond lengths are stretched compared to the corresponding W–O bonds (1.919 and 2.158 Å). We consider that the stretch of the W–X bonds in the C_s-doped (2.076 and 2.168 Å) and N_s-doped (1.956 and 2.128 Å) models may be due to the larger atomic radius of C (0.77 Å) and N (0.70 Å) than that of the O atom (0.66 Å). While in the F_s-doped model, the longer W–F bonds (2.065 and 2.269 Å) may due to the implantation of the F atom arousing an increase of the Coulomb repulsion. The C_i-doped structure (Figure 1e) creates a large lattice distortion, resulting in the reduced coordination of the W atom bound to the C impurity atom. The C atom is inclined to bond with two adjacent lattice O atoms and two lattice W atoms, and the two C–O and W–C bond lengths are 1.362, 1.398, 2.033, and 2.108 Å, respectively. In the N_i-doped model, as shown in Figure 1f, the N impurity atom is bound to the adjacent lattice O, W, and Zn atoms and the resulting N–O, N–Zn, and N–W bonds are 1.360, 2.089, and 1.992 Å, respectively.

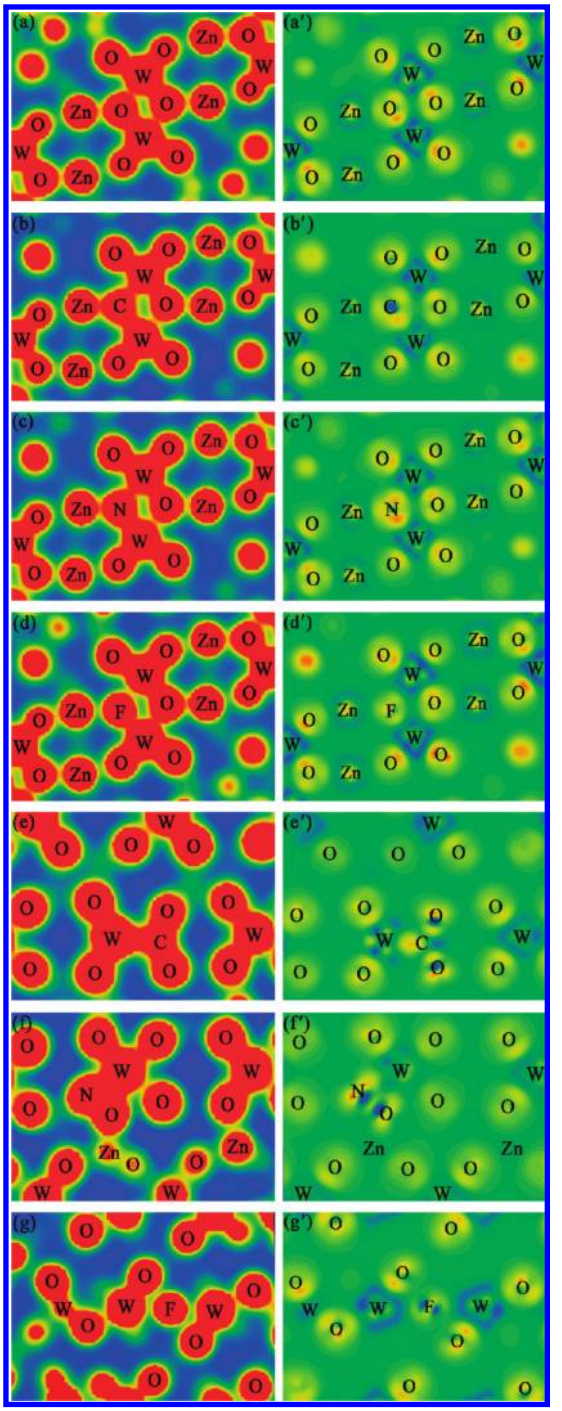

Figure 2. The total electron density maps (left) and the electron difference density maps (right) for (a, a′) pure, (b, b′) C_s-doped, (c, c′) N_s-doped, (d, d′) F_s-doped, (e, e′) C_i-doped, (f, f′) N_i-doped, and (g, g′) F_i-doped $ZnWO_4$.

For the F_i-doped structure in Figure 1g, the F atom bonds with two adjacent lattice W atoms after geometrical optimization, and the F–W bonds are 2.212 and 2.251 Å. We find that the distances between the F impurity and the two nearest O atoms are about 2.032 and 2.446 Å, respectively, which suggests that there may be interactions between F and O atoms in the lattice.

To understand the charge redistribution induced by C, N, and F doping, we calculate the electron density and different density

Table 1. Mulliken Charge Population on the Zn, W, O, C, N, and F Atoms for Pure Phase and Doped Systems

	charge population					
species	Zn	W	O	C	N	F
pure	1.25	1.44	−0.65, −0.70			
C_s	1.11	1.34, 1.38	−0.65, −0.70	−0.52		
C_i	1.22	1.35, 1.38	−0.57, −0.59	−0.02		
N_s	1.20	1.39, 1.41	−0.65, −0.70		−0.63	
N_i	1.22, 1.27	1.45	−0.40		−0.31	
F_s	1.25	1.41, 1.43	−0.65, −0.70			−0.48
F_i	1.25	1.46, 1.47	−0.55, −0.55			−0.38
C_s+2F_s	1.13	1.20, 1.31	−0.65, −0.70	−0.65		−0.49, −0.54
C_i+2N_s	1.23	1.40, 1.41	−0.65, −0.70	0.01	−0.64	
N_s+F_s	1.25	1.44	−0.65, −0.70		−0.71	−0.51
N_i+F_s	1.23, 1.28	1.45	−0.47		−0.37	−0.49

maps for the monodoped $ZnWO_4$ supercell, as shown in Figure 2. For a comparison, the pure $ZnWO_4$ is also plotted. Mulliken charge population analyses are calculated and shown in Table 1. Confessedly, the absolute magnitudes of the atomic charges yielded by the population analysis have little physical meaning, but we can find some useful information from the relative values of Mulliken population. As shown in Figure 2b, b′, c, c′, d, and d′, when the X (X = C, N, and F) atoms substitute for the O atoms, after charge redistribution, the interaction between the X anion and W cations gets weak. The calculated charges on the substitutional X anions (C_s, −0.52*e*; N_s, −0.63*e*; F_s, −0.48*e*) are less than that of the original O ions (−0.70*e*), and the two adjacent W cations have decreased their charge compared with the original W 1.44*e*. Thus, we attribute the weaker W−X bonds to the lesser charge transfer from adjacent W atoms. For the C_i- and N_i-doped structures, the total electron density maps in parts e and f of Figure 2 show the C and N doping atoms bonded with adjacent O atoms are major covalent-like bonding interactions by common electron clouds. Figure 2e′ and f′ shows there are some charges transferring from the lattice O to the bonding impurity atoms. The total charges on O−C−O and N−O are −1.18*e* and −0.71*e*, respectively, indicating that CO_2^- and NO^- species are formed in the C_i- and N_i-doped $ZnWO_4$. In the F_i-doped model (Figure 2g and g′), the doped F ion captures the electrons from adjacent W ions, forming two predominantly ionic F−W bonds. The charges on the F and adjacent W ions are −0.38, 1.46, and 1.47*e*, respectively. Due to the electronegativity of F being higher than that of O, the two adjacent O ions show a charge decrease to −0.55*e* compared with the original −0.65*e*; i.e., some of the charges on the F ion have been obtained from the adjacent O ions.

B. Electronic Structures. To investigate the changes of the electronic structures of the doped $ZnWO_4$ and further study the effect of these changes on determining the photoactivity, the spin band structures and the project density of states (PDOS) of pure and C-, N-, and F-doped $ZnWO_4$ are calculated and shown in Figure 3.

For the pure phase, shown in Figure 3a, the calculated band gap is about 2.88 eV. Experimentally, the pure $ZnWO_4$ has a larger band gap of about 3.69 eV.[47] The band gap underestimation of DFT always exists due to the well-known limitation of predicting accurate conduction band properties.[48] However, it is still a widely accepted method to discuss the valence band in the electronic structure calculations, and this gives a reasonable explanation for the experimental results, because only the relative positions of the occupied states and empty states need be taken into account. As shown in Figure 3a, the valence band maximum (VBM) of the pure $ZnWO_4$ is predominantly contributed to by O 2p character, and the conduction band minimum (CBM) mainly originates from the W 5d and has little O 2p contribution. These results indicate that the electronic transition from O 2p states to W 5d states is responsible for the optical absorption edge.

The incorporation of substituted C and N atoms on lattice O sites induces acceptor states, the position of which is largely determined by 2p orbital energies of the anions, above the VBM of $ZnWO_4$. The neutral 2p orbital energies of C (−5.23 eV) and N (−7.07 eV) are higher than the O 2p orbital energy (−9.03 eV). Therefore, the acceptor levels induced by C_s impurity are deep inside the gap of $ZnWO_4$ (Figure 3b), whereas the N_s acceptor level is relatively shallow (Figure 3c). As the C atom has two less valence electrons than O, the C_s impurity acts as a double acceptor. Similarly, the N_s impurity acts as a single acceptor, showing spin-down character. For the F_s-doped structure, shown in Figure 3d, some levels below the CB pass through the highest occupied level, indicating that substitutial F impurity acts as a donor doping in $ZnWO_4$. Some occupied 5d states of the W atoms adjacent to the F-doping lie below the highest occupied level as a $5d^1$ state. Due to the fact that the substitutional F dopant has a lower 2p orbital energy (−11.12 eV) than the O atom, most of the F 2p states are localized at lower energies, mixing with the valence band states, and no F_s 2p states are situated in the gap.

For the C_i-doped $ZnWO_4$, the characteristic feature in the electronic structure of CO_2 species is the occurrence of two localized π states, with energies just below the O 2p valence band, and two antibonding (π^*) occupied states, whose energies lie in the band gap, as shown in Figure 3e. Although the host band gap has a slight narrowing, the phototransition energy has a larger red shift to about 1.15 eV. Seen from Figure 3f, in the N_i-doped structure, one occupied NO π^* level acts as one gap state, and the other gap state is formed by one partially filled NO π^* state, i.e., for the spin-up bands two isolated NO π^* levels lie in the gap and for the spin-down bands one occupied impurity level lies below the highest occupied level and another unoccupied level lies above the highest occupied level. For the F_i-doped model, two impurity levels, consisting of the mixing of O 2p and F 2p states, appear in the forbidden gap; one locates above the VB for the spin-up channel, and the other lies above the highest occupied level for the spin-down channel, showing unoccupied character.

On the basis of the above calculations and analyses, we conclude that, though the host band gap of the monodoped $ZnWO_4$ has little narrowing, the photon transition energy decreases to varying degrees. However, we must acknowledge the merely redshifting light absorption does not guarantee satisfactory photoactivity. All of these monodoped models, except the C_i-doped $ZnWO_4$, form partially filled states in the band gap, which may act as a trap of the photoexcited electron and thus reduce the photogenerated current. Figure 4 gives the energies of formation of the various doped $ZnWO_4$ considered in this work as a function of the oxygen chemical potential $\Delta\mu_O$, which is a parameter that characterizes the oxygen environment during synthesis. Although in the C_i-doped model no partially filled states formed, from Figure 4, we find that it is difficult to form in the $ZnWO_4$ due to its larger formation energy. Therefore, we

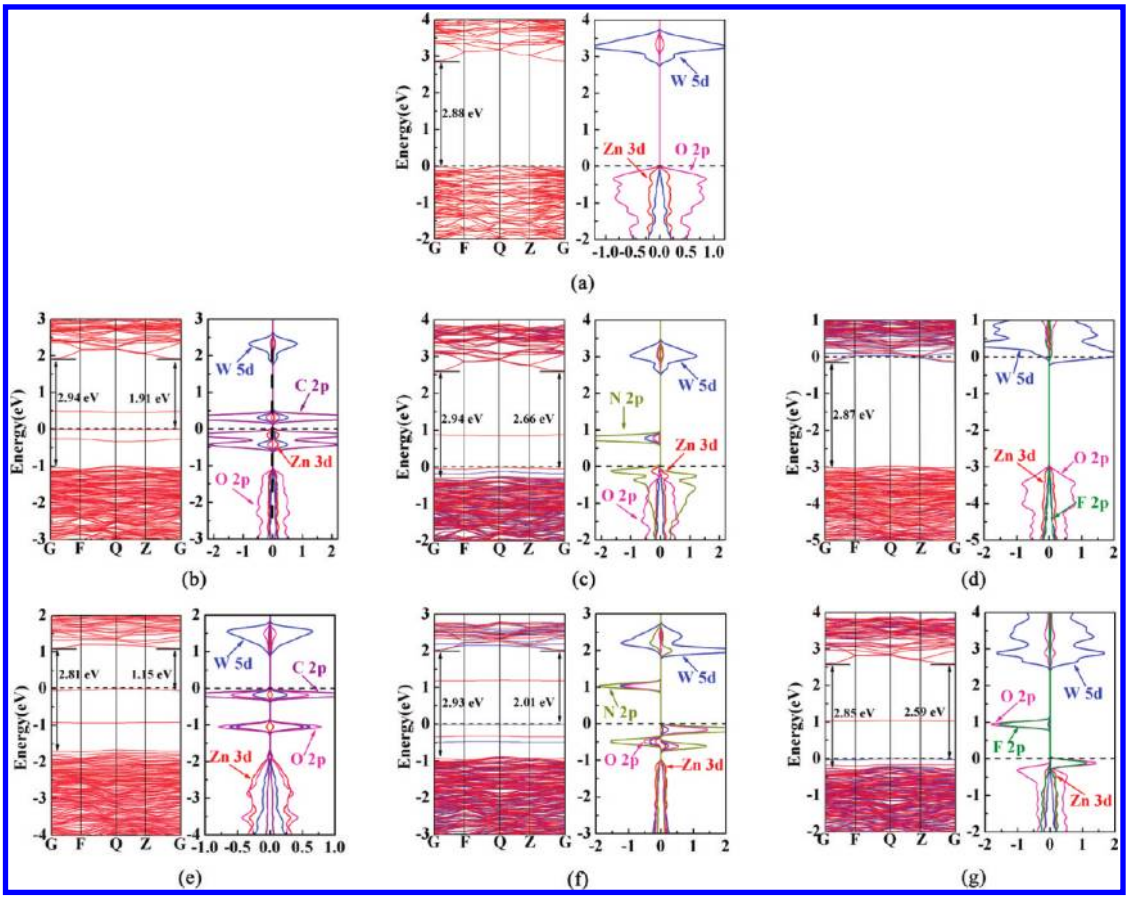

Figure 3. The band structure and projected density of states (PDOS) for monodoped $ZnWO_4$: (a) pure, (b) C_s-doped, (c) N_s-doped, (d) F_s-doped, (e) C_i-doped, (f) N_i-doped, and (g) F_i-doped $ZnWO_4$. The bule and red lines represent the spin up and down channels, respectively. The dashed lines represent the highest occupied level.

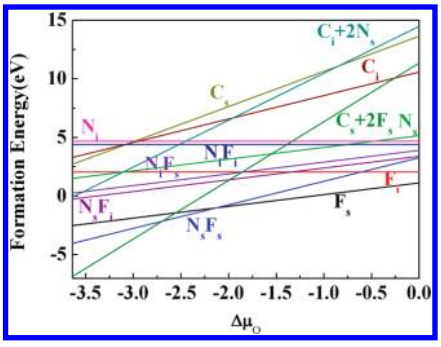

Figure 4. Formation energies (E_{form}, in eV) as a function of $\Delta\mu_O$ (difference in the oxygen chemical potentials) for different monodoped and codoped $ZnWO_4$ configurations: C_s-doped, N_s-doped, F_s-doped, C_i-doped, N_i-doped, F_i-doped, C_s+2F_s-codoped, C_i+2N_s-codoped, N_s+F_s-codoped, N_s+F_i-codoped, N_i+F_s-codoped, and N_i+F_i-codoped models.

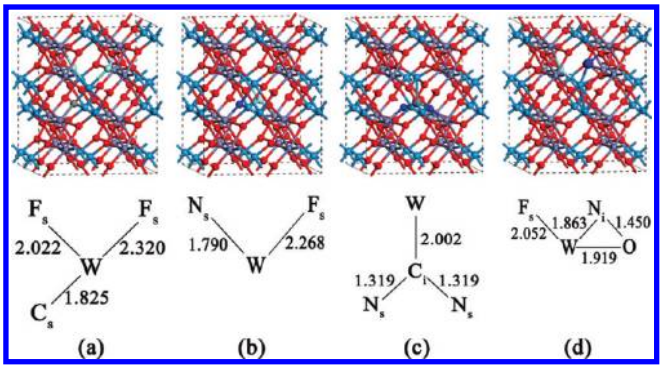

Figure 5. The optimized structures of (a) C_s+2F_s-codoped, (b) N_s+F_s-codoped, (c) C_i+2N_s-codoped, and (d) N_i+F_s-codoped $ZnWO_4$. The partial structures are also shown. The gray, azure, red, dark gray, blue, and pewter spheres represent zinc, tungsten, oxygen, carbon, nitrogen, and fluorine, respectively.

should explore other doping types for $ZnWO_4$, using the synergetic effect of DAP recombination, to decrease the formation energy of doping structure and passivate the related defect bands in the monodoped models.

3.2. (C, F)-, (C, N)-, and (N, F)-Codoped $ZnWO_4$. The above-mentioned monodoped $ZnWO_4$ systems create partially occupied impurity bands that can facilitate the formation of recombination centers, and thus may reduce the photoactivity. Therefore, in this section, the main point is to avoid creating the partially occupied states, using the DAP to adjust the electronic structure of $ZnWO_4$ with the charge compensated effect. On the basis of the above discussions and the electronic configurations of C $2s^22p^2$, N $2s^22p^3$, and F $2s^22p^5$, we think that C_s+2F_s, C_i+2N_s, N_s+F_s, N_s+F_i, N_i+F_s, and N_i+F_i codoping as codopant pairs probably get desirable photoactivity. In all of these cases, the systems still keep semiconductor character, resulting from the electrons on the donor levels

passivating the same amount of holes on the acceptor levels. The optimized structures for N_s+F_i, N_i+F_s, and N_i+F_i codoping are almost the same, and the calculated electronic properties are similar. Thus, in the present work, only the synergistic effects of C_s+2F_s-, C_i+2N_s-, N_s+F_s-, and N_i+F_s-codoped configurations are discussed in detail (the optimized configurations and the electronic structures of N_s+F_i- and N_i+F_i-codoped $ZnWO_4$ are shown in the Supporting Information).

A. Geometric Structures. To investigate the most stable configuration of C_s+2F_s- and N_s+F_s-codoped $ZnWO_4$, several distinct supercell structures with substituted dopants placed at several possible sites are examined. It is found that, in the most stable C_s+2F_s-codoped $ZnWO_4$, two O_b sites are substituted by two F atoms, and the O_a site in the diagonally opposite of one of the two O_b sites bound to the same W atom is replaced by one C atom, as shown in Figure 5a. The two F−W bonds are stretched to 2.022 and 2.320 Å compared with the original O−W bonds 1.807 Å, and the C−W bond is shrunk from 2.158 to 1.807 Å with respect to the corresponding O−W bond in pure $ZnWO_4$. After geometry optimization, the most stable N_s+F_s-codoping model (Figure 5b) is the structure in which N and F atoms are replacing the two farthest O_a atoms bound to the same W atom, respectively. The two optimized F−W bonds and one F−Zn bond are stretched to 2.229, 2.268, and 2.115 Å, while the two N−W bonds and one N−Zn bond are shrunk to 2.161, 1.790, and 1.990 Å, according to the two original O−W bonds and one O−Zn bond 1.919, 2.158, and 2.075 Å, respectively. The formation energies for the C_s+2F_s- and N_s+F_s-codoped configuration are also shown in Figure 4, which are smaller than that of mono C_s- and N_s-doped $ZnWO_4$.

The optimized configuration of C_i+2N_s-codoped $ZnWO_4$ (Figure 5c) is similar to the mono C_i-doping system, with reduced coordination of the W atom bound to the C impurity occurring due to a large lattice distortion. The two nearest O_a atoms bound to the same W atom are substituted by two N atoms, and the C_i impurity atom is inclined to bond with them, resulting in forming two same N−C bonds and one C−W bond. The lengths of N−C and C−W bonds are shrunk to 1.319 and 2.002 Å compared with the corresponding O−C and C−W bonds in the C_i-doping system. In the N_i+F_s-codoping system (Figure 5d), the F atom replaces one lattice O_b, while the N_i impurity forms the N−O species with the other lattice O_b atom bound to the same W atom. The resulting N−O bond length is 1.450 Å, which is longer than the N−O bond in the mono N_i-doped $ZnWO_4$. As shown in Figure 4, the formation energy of C_i+2N_s-codoped $ZnWO_4$ is smaller than the mono C_i-doped model when $\Delta\mu_O < -1.9$ eV, while the formation for N_i doping becomes easier as implantation of F_s impurity.

We calculated the defect pair binding energy of the codoped $ZnWO_4$ supercell according to $E_b = E(D_1) + E(D_2) - E(D_1+D_2) - E(ZnWO_4)$[49] to determine whether the defect pairs are stable. Here, $E(D)$ is the total energy of the doped system calculated with the same supercell. If the defect pairs tend to bind to each other when both are present in the sample, E_b will be a positive value, and of course it is the same in reverse. The calculated binding energies E_b for the (C_s+2F_s), (N_s+F_s), (C_i+2N_s), and (N_i+F_s) pairs are 4.85, 3.05, 6.43, and 1.93 eV, respectively, indicating that the pairs are more stable than the isolated impurities. We attribute the large binding energy to charge transfer from donors to acceptors and the associated strong Coulomb interaction between positively charged donors and negatively charged acceptors.

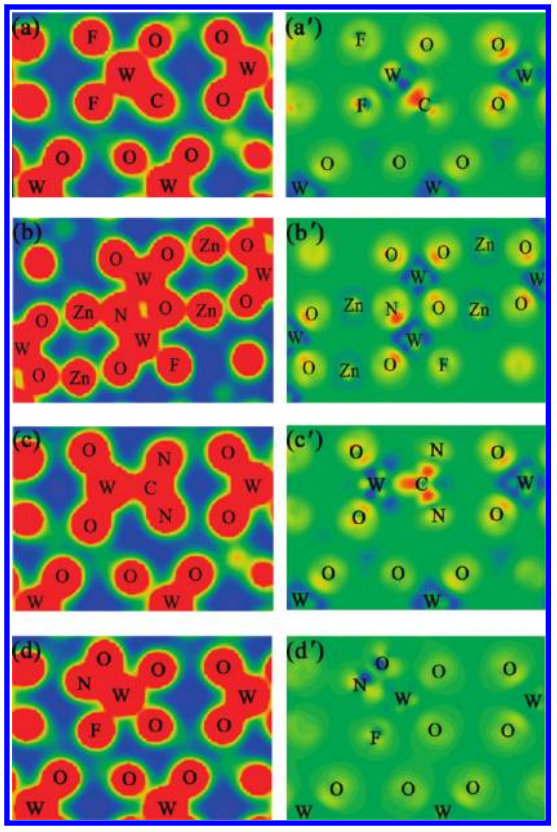

Figure 6. Total electron density maps (left) and electron difference density maps (right) for (a, a′) C_s+2F_s-codoped, (b, b′) N_s+F_s-codoped, (c, c′) C_i+2N_s-codoped, and (d, d′) N_i+F_s-codoped $ZnWO_4$.

After electronic redistribution, there must be some significant changes of the chemical bonds in the codoping systems. In order to study more about these changes of chemical bonds due to the codoping, the electron density and electron density difference maps are given in Figure 6. For C_s+2F_s- and N_s+F_s-codoped $ZnWO_4$, as shown in parts a and b of Figure 6, there are common electron clouds around the C−W and N−W bonds and the population on these two bonds are 1.17 and 1.02*e*, indicating the C−W and N−W bonds showing major covalent-like bonding character. Figure 6a′ and b′ show there are some charges transferring from the lattice W to the bonding C and N impurity atoms. For the C_s+2F_s-codoping system, the charges on W, C, and two F atoms are 1.20, −0.65, −0.54, and −0.49*e*, while the charges on W, N, and F atoms are 1.44, −0.71, and −0.51*e* in the N_s+F_s-codoped $ZnWO_4$. In both of the C_s+2F_s- and N_s+F_s-codoping cases, the F atom acts as a single donor, leading to formation of the W $5d^2$ and $5d^1$ state, and these electrons passivate the same amount of holes on the C and N impurities, which act as a double and a single acceptor, respectively.

From part c′ of Figure 6, we can find that some charges transfer from the C atom to the adjacent N atoms, indicating the C_i impurity acts as a double donor and the two N_s atoms act as two single acceptors. Spontaneously, the two 2p electrons brought by the C dopant pair up with the two unpaired N 2p electrons in the $ZnWO_4$ lattice. Interestingly, we also find that there are some charges transferring between the W and C atoms. The reason for this phenomenon is that, due to changing of the coordination of the lattice W atom from hexa-coordination to tetra-coordination, the W atom transfers the two extra electrons to the C_i atom. The

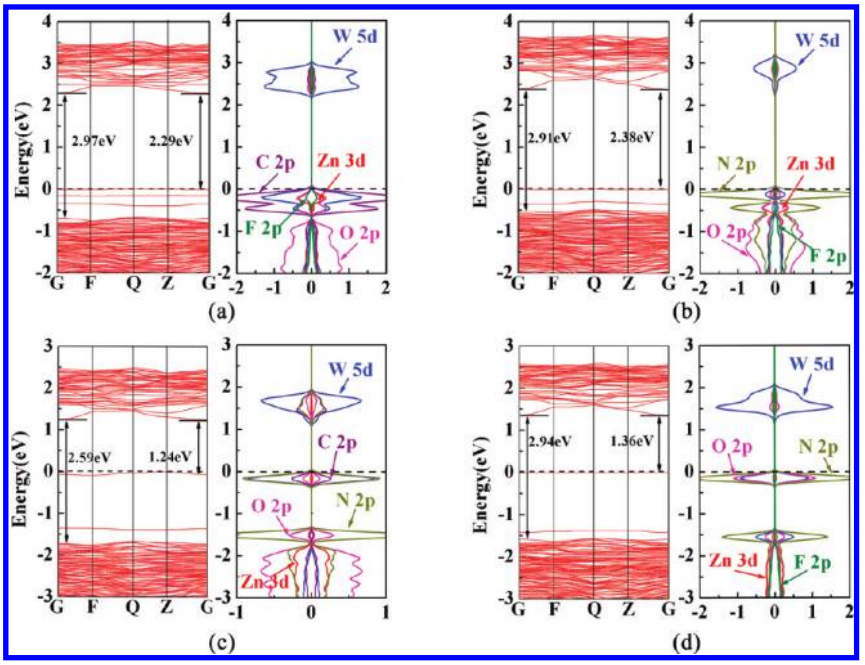

Figure 7. Band structure and projected density of states (PDOS) for codoped $ZnWO_4$: (a) C_s+2F_s-codoped, (b) N_s+F_s-codoped, (c) C_i+2N_s-codoped, and (d) N_i+F_s-codoped $ZnWO_4$. The dashed lines represent the highest occupied level.

calculated charges on the C impurity are 0.01*e*, close to 0, indicating the C atom almost keeps the neutral character, which is in good agreement with the above conclusion. For the N_i+F_s-codoped structure, the total electron density map in Figure 6d shows the N doping atom bonded with adjacent O is a major covalent-like bonding interaction by common electron clouds. Figure 6d′ shows there are some charges transferring between the lattice O and the N impurity atom. The total charges on N−O are −0.84*e*, indicating that a NO^- species is formed in this doped type of $ZnWO_4$. In this case, the F_s acts as a single donor, and the extra electron on the W $5d^1$ state passivates the hole on the NO π^* level. Namely, the electrons brought by the donor passivate the same amount of holes on the acceptor level, so that all of these codoped $ZnWO_4$ systems can still be of semiconductor character.

B. Electronic Structures. From the band structures and PDOS of the four codoped $ZnWO_4$ in Figure 7, we can see that the highest occupied levels are pinned above the impurity levels, indicating no partially occupied states induced by codoping, showing a passivated characteristic, and the W 5d states are mainly contributing to the conduction band. In the present calculations for C_s+2F_s- and N_s+F_s-codoping systems, no band gap narrowing is predicted, as shown in Figure 7a and b, respectively. For the C_s+2F_s-codoping system, three impurity levels are localized in the band gap and the PDOS shows that the impurity levels predominantly originate from the C 2p states with input from the W 5d states, resulting in the electron excitation energy from the highest impurity level to the CBM being about 2.29 eV. For N_s+F_s-codoped $ZnWO_4$, there are only two impurity levels in the band gap. The PDOS of the N_s+F_s-codoped model shows that the N 2p and F 2p states mix with O 2p states in the whole valence band, while the top of the valence band is mainly composed by the N 2p and O 2p states, which should be attributed to the lower 2p orbital energy of the F atom than the N 2p and O 2p orbitals. However, the impurity levels in the gap predominantly originate from the N 2p states, and the transition energy from the higher N 2p gap states to the CBM is about 2.38 eV.

The host band gap of the C_i+2N_s-codoping system (Figure 7c) has a slight decrease to about 2.59 eV, and two impurity levels are localized in the band gap. The transition energy from the gap states to CBM is about 1.24 eV. From the PDOS, we can see that the impurity levels mainly originate from the N 2p mixing with W 5d with little input from the C 2p states. For the N_i+F_s codoping in Figure 7d, the calculated band structure indicates that the host band gap has no significant narrowing and also two impurity levels localized in the gap. The PDOS shows that the levels in the gap mostly originate from the N 2p and O 2p states mixing with W 5d states, which confirms the existence of NO^- species as previously mentioned. The transition energy from the higher impurity states to the CBM is about 1.36 eV. By consideration of a scissor operator of 0.81 eV to correct the calculated gap of pure $ZnWO_4$ to the experimental value of 3.69 eV, the transition energy of C_i+2N_s- and N_i+F_s-codoping systems from the gap states to CBM should be about 2.05 and 2.17 eV, corresponding to 605 and 572 nm visible-light absorption. In addition, the top of the valence band in these two codoped models has a shift to the lower energy, suggesting the oxidation ability of the valence band hole carriers induced by the photoexcited electrons may be enhanced, thus further improving the photocatalytic activity of $ZnWO_4$.

The above discussions of these four systems clearly indicate a decrease of formation energy for dopant implantation and a red shift of the optical absorption especially in both of the C_i+2N_s- and N_i+F_s-codoping systems. Moreover, in all of these codoping systems, the fully occupied states, which are formed by the compensate effects between the DAP, appear in contrast to monodoping (partially occupied states); these fully occupied states in the valence band edge cannot act as recombination centers. Therefore, the photocurrent density of codoped $ZnWO_4$ under both UV and visible-light radiation will be improved.

4. CONCLUSIONS

The electronic properties of C, N, and F monodoped and pairwise codoped $ZnWO_4$ have been studied by means of first-principles DFT calculations. The monodoping systems do not possess favorable characteristics to improve the photoactivity of $ZnWO_4$ despite their photon transition energy decreasing to varying degrees; partially occupied gap states are introduced into the band gap, which could serve to act as effective recombination centers. In the codoping systems, we find that the formation energy of codoping structures is decreased and the related defect bands in the monodoped models are passivated by using the synergetic effect of DAP recombination. In both of the C_s+2F_s- and N_s+F_s-codoping cases, the F atom acts as a single donor, leading to formation of the W $5d^2$ and $5d^1$ state, and these electrons passivate the same amount of holes on the C and N impurities, which act as a double and a single acceptor, respectively. The electron excitation energy from the impurity states to the CBM decreases by about 0.6 and 0.5 eV, respectively, while no narrowing of the host band gap is present. In the C_i+2N_s-codoped $ZnWO_4$, our calculations indicate the charge compensation effect in the N−C−N species, i.e., the acceptor−donor−acceptor species. For the N_i+F_s-codoped $ZnWO_4$, the F_s act as a single donor and the extra electron on the W $5d^1$ state passivates the hole on the NO π^* level. Both the C_i+2N_s- and N_i+F_s-codoped $ZnWO_4$ reduce the electron transition energy from the impurity levels to the CBM to the ideal visible-light region; therefore, the C_i+2N_s codoping decreases the host band gap of $ZnWO_4$ by about 0.3 eV. Our work provides a solid basis for identifying a "good pair" between C, N, and F atoms in the $ZnWO_4$ system, and shows that codoping with C_i+2N_s and N_i+F_s will be promising ways for improving the visible-light photoactivity of wide band gap semiconductor photocatalysts.

■ ASSOCIATED CONTENT

Supporting Information. The optimized structure, band structures, and PDOS of N_s+F_i- and N_i+F_i-codoped $ZnWO_4$. This material is available free of charge via the Internet at http://pubs.acs.org.

■ AUTHOR INFORMATION

Corresponding Author

*Phone: 86-531-88366330. Fax: 86-531-88365174. E-mail: fwl@sdu.edu.cn.

■ ACKNOWLEDGMENT

This work is supported by the National Natural Science Foundation of China (Grant Nos. 50802056 and 91022034), 973 Program of China (Grant No. 2009CB930103), Excellent Youth Foundation of Shandong Scientific Committee (Grant No. JQ201015), Youth Scientist (Doctoral) Foundation of Shandong Province of China (Grant No. BS2009CL038), and Independent Innovation Foundation of Shandong University (Grant No. 2009TS016).

■ REFERENCES

(1) Linsebigle, A. L.; Lu, G. Q.; Yates, J. T. *Chem. Rev.* **1995**, *95*, 735.
(2) Yu, C. L.; Yu, J. C.; Chan, M. *J. Solid State Chem.* **2009**, *182*, 1061.
(3) Yu, C. L.; Yu, J. C. *Catal. Lett.* **2009**, *129*, 462.
(4) Herrmann, J. M.; Disdier, J.; Pichat, P. *Chem. Phys. Lett.* **1984**, *108*, 618.
(5) Choi, W.; Termin, A.; Hoffmann, M. R. *J. Phys. Chem.* **1994**, *98*, 13669.
(6) Couselo, N.; García, F. G.; Candal, R. J.; Jobbágy, M. J. *PhysChemComm* **2008**, *112*, 1094.
(7) Yang, Y.; Wang, H. Y.; Li, X.; Wang, C. *Mater. Lett.* **2009**, *63*, 331.
(8) Long, R.; Dai, Y.; Huang, B. B. *J. Phys. Chem. C* **2009**, *113*, 650.
(9) Long, R.; Dai, Y.; Huang, B. B. *Comput. Mater. Sci.* **2008**, *42*, 161.
(10) Asahi, R.; Morikawa, T.; Ohwaki, T.; Aoki, K.; Taga, Y. *Science* **2001**, *293*, 269.
(11) Irie, H.; Watanabe, Y.; Hashimoto, K. *J. Phys. Chem. B* **2003**, *107*, 5483.
(12) Umebayashi, T.; Yamaki, Y.; Itoh, H.; Asai, K. *Appl. Phys. Lett.* **2002**, *81*, 454.
(13) Chen, D.; Yang, D.; Wang, Q.; Jiang, Y. *Ind. Eng. Chem. Res.* **2006**, *45*, 4110.
(14) Sakthivel., S.; Kisch, H. *Angew. Chem., Int. Ed.* **2003**, *42*, 4908.
(15) Zhao, X.; Zhu, Y. F. *Environ. Sci. Technol.* **2006**, *40*, 3367.
(16) Lin, J.; Lin, J.; Zhu, Y. F. *Inorg. Chem.* **2007**, *46*, 8372.
(17) Fu, H. B.; Lin, J.; Zhang, L. W.; Zhu, Y. F. *Appl. Catal., A* **2006**, *306*, 58.
(18) Huang, G. L.; Zhu, Y. F. *J. Phys. Chem. C* **2007**, *111*, 11952.
(19) Huang, G. L.; Zhang, S. C.; Xu, T. G.; Zhu, Y. F. *Environ. Sci. Technol.* **2008**, *42*, 8516.
(20) Chen., S. H.; Sun, S. X.; Sun, H. G.; Fan, W. L.; Zhao, X.; Sun, X. *J. Phys. Chem. C* **2010**, *114*, 7680.
(21) Sun., H. G.; Fan, W. L.; Li, Y. L.; Cheng, X. F.; Li, P.; Zhao, X. *J. Solid State Chem.* **2010**, *183*, 3052.
(22) Srinivasan, S. S.; Wade, J.; Stefanakos, E. K.; Goswami, Y. *J. Alloys Compd.* **2006**, *424*, 322.
(23) Cong, Y.; Zhang, J. L.; Chen., F.; Anpo., M.; He., D. N. *J. Phys. Chem. C* **2007**, *111*, 10618.
(24) Mi, L.; Xu, P.; Shen, H.; Wang, P. N.; Shen, W. D. *Appl. Phys. Lett.* **2007**, *90*, 171909.
(25) In, S.; Orlov, A.; Berg, R.; Garcia, F.; Pedrosa-Jimenez, S.; Tikhov, M. S.; Wright, D. S.; Lambert, R. M. *J. Am. Chem. Soc.* **2007**, *129*, 13790.
(26) Gombac, V.; De Rogatis, L.; Gasparotto, A.; Vicario, G.; Montini, T.; Barreca, D.; Balducci, G.; Fornasiero, P.; Tondello, E.; Graziani, M. *Chem. Phys.* **2007**, *339*, 111.
(27) Li, D.; Haneda, H.; Hishita, S.; Ohashi, N. *Chem. Mater.* **2005**, *17*, 2588.
(28) Li, D.; Haneda, H.; Hishita, S.; Ohashi, N. *Chem. Mater.* **2005**, *17*, 2596.
(29) Li, D.; Ohashi, N.; Hishita, S.; Kolodiazhnyi, T.; Haneda, H. *J. Solid State Chem.* **2005**, *178*, 3293.
(30) Cong, Y.; Chen, F.; Zhang, J. L.; Anpo, M. *Chem. Lett.* **2006**, *35*, 800.
(31) Di Valentin, C.; Finazzi, E.; Pacchioni, G. *Chem. Mater.* **2008**, *20*, 3706.
(32) Di Valentin, C.; Pacchioni, G.; Onishi, H.; Kudo, A. *Chem. Phys. Lett.* **2009**, *469*, 166.
(33) Long, R.; English, N. J. *Appl. Phys. Lett.* **2009**, *94*, 132102.
(34) Long, R.; English, N. J. *Chem. Phys. Lett.* **2009**, *478*, 175.
(35) Dvoranova, D.; Brezova, V.; Mazur, M.; Malati, M. A. *Appl. Catal., B* **2002**, *37*, 91.
(36) Yong, L.; Fu, P. F.; Dai, X. G.; Du, Z. W. *Prog. Chem.* **2004**, *16*, 738.
(37) Khan, S. U. M.; Al-shahry, M.; Ingler, W. B., Jr. *Science* **2002**, *297*, 2243.
(38) Huang, D. G.; Liao, S. J.; Liu, J. M.; Dang, Z.; Petrik, L. *J. Photochem. Photobiol., A* **2006**, *184*, 282.
(39) Murugananandham, M.; Kusumoto, Y. *J. Phys. Chem. C* **2009**, *113*, 16144.
(40) Sun, H. G.; Zhao, X.; Zhang, L.; Fan, W. L. *J. Phys. Chem. C* **2011**, *115*, 2218.
(41) Bergman, P.; Ying, G.; Monemar, B.; Holta, P. O. *J. Appl. Phys.* **1987**, *61*, 4589.

(42) Segall, M. D.; Lindan, P. J. D.; Probert, M. J.; Pickard, C. J.; Hasnip, P. J.; Clark, S. J.; Payne, M. C. *J. Phys.: Condens. Matter* **2002**, *14*, 2717.
(43) Perdew, J. P.; Chevary, J. A.; Vosko, S. H.; Jackson, K. A.; Pederson, M. R.; Singh, D. J.; Fiolhais, C. *Phys. Rev. B* **1992**, *46*, 6671.
(44) Perdew, J. P.; Burke, K.; Ernzerhof, M. *Phys. Rev. Lett.* **1996**, *77*, 3865.
(45) Vanderbilt, D. *Phys. Rev. B* **1990**, *41*, 7892.
(46) Monkhorst, H. J.; Pack, J. *Phys. Rev. B* **1976**, *13*, 5188.
(47) Lin, J; Lin, J.; Zhu, Y. F. *Inorg. Chem.* **2007**, *46*, 8372.
(48) Martin, R. M. *Electronic Structure: Basic Theory and Practical Methods*; Cambridge University Press: Cambridge, England, 2004.
(49) Gai, Y. Q.; Li, J. B.; Li, S. S.; Xia, J. B.; Wei, S. H. *Phys. Rev. Lett.* **2009**, *102*, 036402.